Heliyon 6 (2020) e04733

Contents lists available at ScienceDirect

Heliyon

journal homepage: www.cell.com/heliyon

Research article

9-phenyl acridine photosensitizes A375 cells to UVA radiation

Surajit Hansda [a], Gargi Ghosh [b], Rita Ghosh [a,*]

[a] Department of Biochemistry & Biophysics, University of Kalyani, Kalyani, 741235, West Bengal, India
[b] Department of Molecular Biology & Biotechnology, University of Kalyani, Kalyani, 741235, West Bengal, India

ARTICLE INFO

Keywords:
Cell biology
Biochemistry
Molecular biology
Cancer research
Toxicology
9-phenyl acridine
A375 cells
Photosensitization
ROS
DNA damage
Apoptosis

ABSTRACT

Acridines are an important class of bioactive molecules having varied uses. Its derivative, 9-phenylacridine (ACPH) had been found to exhibit antitumor activity both in cell lines and *in vivo* model. Its DNA binding ability and absorbance in the ultraviolet range encouraged us to investigate its role as a photosensitizer with UVA radiation. We investigated the effects of ACPH prior to UVA exposure on *in vitro* DNA through photo-cleavage assay. Effect of such treatment was also studied in cultured A375 melanoma cells. Endpoints studied included morphological changes, evaluation of cellular viability, scratch assay, intracellular reactive oxygen species (ROS) production, DNA damage, lipid peroxidation, glutathione (GSH) level, autophagy, cell cycle progression, depletion of mitochondrial membrane potential ($\Delta\Psi mt$), induction of apoptosis and Hoechst dye efflux assay. Our findings indicated that ACPH could sensitize damage to DNA induced by UVA both *in vitro* and in cells. It could also potentiate cell killing by UVA. It arrested cells in G_2/M phase and induced apoptotic death through mitochondria mediated pathway. This sensitization was through enhancement of intracellular ROS. Our findings also indicated that the stem cells side population was reduced on such treatment. The findings are important as it indicates ACPH as a promising photosensitizer and indicates its possible role in photodynamic therapy.

1. Introduction

Derivatives of acridine are well known for their therapeutic benefits. A number of acridines have been found to be of use as antiprotozoan, antibacterial or anticancer agents [1, 2, 3, 4, 5]. Our earlier works have revealed that 9-phenyl acridine (ACPH) exhibited anticancer activity in cell lines and also *in vivo* animal model [6]. Bioinformatics studies have indicated that it could have topoisomerase I inhibitory activity [7]. It could also act as a PARP 1 inhibitor [8, 9] and was very effective in combination with cisplatin in cell line-based assays [10]. ACPH also satisfied all criteria for a candidate drug from Lipinski rule [8], and also shown good uptake in cells (data not shown here).

Photosensitizing activity has been observed in a number of acridine derivatives [11, 12]. In fact, way back in 1900 the lethal effect of combination of light with acridine was first observed by Oscar Raab [13]. As ACPH has the ability to bind to DNA and also has absorbance in the UVA range [14], its photosensitizing activity is worth evaluation.

Use of sunlight, either alone or in combination with other compounds have been utilized in traditional medicine for different dermal disorders including cancer, which was known as heliotherapy [15, 16]. Psoralen plus UVA (PUVA) therapy is still one of the well established treatment for cutaneous cancer, psoriasis and other diseases [15]. Different derivatives of psoralen, like 8-methoxypsoralen are also very effective as photosensitizers [17]. Many other photosensitizers are known that produce reactive oxygen species (ROS) from their dynamic interaction with light; this is known as photodynamic action [18, 19, 20]. A number of photosensitizers including 5-aminolevulinic acid (5-ALA), methyl-aminolevulinate, porfirmer sodium and such other, which act with either visible or UV light, that have been approved for clinical applications [21, 22]. Therapeutic benefits derived from such agents that utilize photodynamic action are known as photodynamic therapy (PDT). The beauty of PDT is its local action at targeted site without adverse systemic effects; it is therefore a popular and alternative option not only for dermatological disorders like vitiligo and psoriasis but also for squamous, basal, hepatocellular and cervical cell carcinoma [22, 23, 24, 25, 26].

Melanoma is one of the most aggressive forms of skin cancer with high mortality due to its poor prognosis. It is refractory to traditional chemotherapy and radiotherapy due to resistance to apoptosis [27, 28]. ACPH alone was effective in A375 melanoma cell line [29]. We have evaluated the photosensitizing potential of ACPH in A375 cells as a model system.

* Corresponding author.
E-mail address: rghosh_bcbp@klyuniv.ac.in (R. Ghosh).

https://doi.org/10.1016/j.heliyon.2020.e04733
Received 29 May 2020; Received in revised form 29 July 2020; Accepted 12 August 2020

The photocleavage activity of ACPH and UVA light was first studied *in vitro* plasmid DNA. The effect of pretreatment with a nontoxic dose of ACPH was studied in cultured melanoma A375 cells and in HEK 293 normal embryonic kidney cells. Different cellular parameters investigated included morphological changes, viability, scratch assay, generation of ROS, DNA damage, lipid peroxidation, GSH level, autophagy, cell cycle arrest, induction of apoptosis, involvement of mitochondria in such process, expression of mitochondrial proapoptotic protein like Bax. Considering the potential use of photosensitizers in PDT for cancer, the importance of ACPH could be likely. Current studies have revealed that cancer cells include a small population of stem-like cells, which make them refractory to treatment because of their ability to purge out drugs. Effect of ACPH and UVA on "cancer stem-like cells" (CSCs) side population was also estimated to evaluate its possible benefit.

2. Materials and methods

2.1. DNA photo-cleavage experiments

The cleavage of pUC19 DNA (0.2 μg) was studied in 1% agarose gel, where electrophoresis was done for 1 hr at 50 V using 1X TAE (Tris-acetate EDTA) running buffer (pH 8.3) [30]. For DNA photo-cleavage studies, the reactions were carried out under UVA light (Philips, 9W lamp, dose rate 6.198 J/m-1/s). The experiments were performed in a total volume of 20 μl that contained plasmid DNA (0.2 μg) in 50 mM Tris HCl buffer (pH 7.2) with 50 mM NaCl; according to the need of the experiment, ACPH (8 μM) was present. Then, the samples were irradiated with UVA light (15 KJ/m^2) and analyzed for the photo-cleaved product formation in gel electrophoresis. 1X Purple loading dye (#B7024S; NEB) was mixed with each reaction mixture. The agarose gel was stained with ethidium bromide (EtBr) (0.2 μg/ml) after the run, visualized and photographed using ChemDoc™ in Bio-Rad XRS+.

2.2. Cell culture

A375 human melanoma cells were cultured in minimal essential media (MEM) (HiMedia) and HEK 293 normal embryonic kidney cells in Dulbecco's modified eagle medium (DMEM) (HiMedia), supplemented with fetal bovine serum (HiMedia) (10%). Cells were routinely maintained in an exponential grown state by growing them at 37 °C in a humidified 5% CO_2 atmosphere through sub-culture in tissue culture grade plasticware (Tarson).

2.2.1. Treatment protocol

Exponentially growing cells were treated with or without a nontoxic dose of ACPH {2 μM, 1hr in phosphate-buffered saline (PBS)}, rinsed in PBS and then exposed to UVA light (15 KJ/m^2) (Philips, 9W lamp, dose rate 6.198 J/m-1/s). After treatment, cells were again rinsed in PBS and either processed immediately or grown in fresh medium according to the need of the experiment.

2.3. Morphological observation

Morphology of control and UVA treated cells without or with ACPH pretreatment were observed immediately after exposure under an inverted microscope (AxioScope AI of Carl Zeiss) and photographed at 10x and 40x magnifications. For A375 cells, morphological changes were also observed under a scanning electron microscope (SEM) (ZEISS EVO LS 10). Samples were dehydrated with graded concentrations of ethanol prior to observation in SEM [31].

2.4. Cell viability assay

Viability was estimated as described earlier from MTT (3-(4, 5-dimethylthiazol-2-yl)-2, 5-diphenyltet-razolium bromide) assay [6]. After treatment, cells were incubated in the dark with MTT (50 μg mL^{-1}) for 2 hrs. The mitochondrial dehydrogenases of viable cells cleave the tetrazolium ring to reduce it to insoluble formazan crystals, which were then dissolved in DMSO. The absorbance of the resulting purple solution was determined at 570 nm by spectrophotometry. The amount of formazan formed depends upon the presence of viable cells to indicate the surviving population of cells. Surviving fraction (S.F.) was expressed as

$$\text{S.F.} = \frac{(\text{O.D.}_{\text{control}} - \text{O.D.}_{\text{treated}})}{\text{O.D.}_{\text{control}}}$$

2.5. Scratch assay

A375 cells were grown in 35 mm plates until about 80–90% confluency and treated according to the treatment protocol. 200 μL plastic pipette tips were used to create a scratch/wound in the culture monolayer of the treated cells. Axioscope fluorescent microscope (Axioscope 2 Plus, Carl Zeiss) was used to measure and photograph the cell regrowth from the wound/scratch edge after 0, 24 and 48 hrs by default settings for all samples [32].

2.6. Determination of intracellular ROS generation

The intracellular ROS generation was evaluated by 2′,7′-dichlorofluorescin diacetate (DCFH-DA) assay through flow cytometry (FACS) (BD Biosciences, USA) and by fluorescence microscopy (AxioScope AI of Carl Zeiss) as described earlier [33]. The cells were treated and rinsed in PBS and incubated for 15 mins at room temperature with 10 μM DCFH-DA (Sigma, USA). DCFH-DA penetrates the cell membranes and is hydrolyzed by intracellular esterases to form dichlorofluorescin (DCFH). DCFH reacts with the intracellular ROS generated to produce the highly fluorescent 2′,7′-dichlorofluorescein (DCF) (λ_{ex}-485 nm, λ_{em}-535 nm). The fluorescence of DCF found in cells was a measure of oxidative damage, which was estimated through flow cytometry FACS Calibur (BD Biosciences, USA) in channel FL-1 for 10,000 cells per sample. DCF fluorescence from cells was also visualized under a fluorescence microscope (AxioScope AI of Carl Zeiss).

2.7. Determination of cellular GSH level in cells

Cellular GSH was estimated from the total soluble thiol present in cells following Ghosh et. al [34]. After treatment, cells were trypsinised, suspended in PBS and centrifuged at 2000 rpm at room temperature. The cell suspension was lysed by three cycles of freezing and thawing. The lysate was centrifuged at 3000 rpm (4 °C). The clear supernatant was collected after precipitation of the cell lysate with 10% sulfosalicylic acid. The total soluble thiol was estimated by intensity of the supernatant with 0.4 mM 5,5′-dithiobis 2 nitrobenzoic acid (DTNB) that was dissolved in 0.2 M sodium phosphate buffer (pH 8.0) and absorbance was read at 412 nm.

2.8. DNA damage assay by flow cytometry

DNA damage can be assayed through flow cytometry after staining with propidium iodide (PI). The fluorescence of cells treated with PI is proportional to the DNA content in the cells present in the different phases of the cell cycle. Normal cells exhibited two populations, cells in G_2/M phase contains 4n number of chromosomes showing the higher fluorescence and the cells in G_1/S phase with 2n number of chromosomes fluorescing with lower intensity. The fluorescence intensity in the hypodiploid population represents the cells with fragmented DNA. There is an increase in the fluorescence of hypo-diploid cell population on increase in DNA damage [35]. In this experiment, hydrogen peroxide (H_2O_2) treatment (600 μM, 1 hr) was used as positive control. After the treatment, cells were trypsinized immediately and centrifuged. The cell pellet was suspended in PBS and fixed in 70% chilled ethanol and kept at 4 °C for 1 hr. To remove RNA, the fixed cells were centrifuged (2500 rpm,

5 mins) at 4 °C and treated with RNase A (Sigma) (10 μg/ml) for 45 mins at 37 °C. Cells were next stained with PI (Sigma) (10 μg/ml) at room temperature for 30 mins [33]. Fluorescence for 10,000 cells per sample was estimated in FL-2 channel of FACS Calibur (BD Biosciences, USA) and analyzed using the Flowing software.

2.9. Lipid peroxidation assay

Lipid peroxidation is determined from the amount of malondialdehyde (MDA) which is found due to lipid peroxidation of the cellular membranes. MDA was determined with thiobarbituric acid as described earlier [34]. After treatment, cells were trypsinized and counted after suspending them in PBS. The cellular extract from 2×10^6 cells in 1 mL was mixed with cold trichloroacetic acid (10% wt⁄vol) in 2 mL and then centrifuged (6000 rpm, 10 mins). 0.67% (wt⁄vol) thiobarbituric acid was added to the pellet in equal volume and incubated for 1 h in a boiling water bath. The O.D. the of supernatant was determined at 535 nm. The amount of MDA found was estimated in nM h^{-1} 10^{-6} cells at 37 °C using the value of molar extinction coefficient as 1.56×10^5 M^{-1} cm^{-1}.

2.10. Determination of the cell cycle by flow cytometry

The cell cycle analysis was performed through flow cytometry (FACS Calibur) (BD Biosciences, USA) on staining with PI as described earlier [34]. In order to determine the distribution of cell population in different phases of the cell cycle, after the treatment, cells were trypsinized immediately or after 6, 16 and 24 hrs treatment and fixed in 70% ethanol at 4 °C for overnight. The cell pellet was then suspended in PBS after centrifugation at 2500 rpm for 5 mins at 4 °C and treated with RNase A (10 μg/ml) (Sigma, USA) dissolved in PBS for 15 mins at room temperature. Finally, the cells were incubated in the dark with 10 μg/ml of PI (Sigma, USA) for 15 mins at room temperature. 10,000 events per sample were sorted and analyzed using Flowing software.

2.11. Detection of autophagy

Autophagy in cells is distinguished by the formation of acidic vesicular organelles (AVOs). Acridine Orange (AO) being weakly basic gets accumulated the acidic compartments showing bright red fluorescence whereas the cytoplasm fluoresces bright green and the nucleolus fluoresces dim red. The volume of the cellular acidic compartment can be quantified from the intensity of the red fluorescence. Treated cells were harvested in cold PBS 24 hrs after treatment and incubated with 1 μg/ml AO (Sigma Aldrich) for 30 min at room temperature. The cells were then observed under the microscope (Invitrogen EVOS FL Auto Cell Imaging System) [36]. For quantification, green (510–530 nm) and red (650 nm) fluorescence emission from 10,000 cells illuminated with blue (488 nm) excitation light was measured with FACS Calibur (BD Biosciences, USA) using Flowing software [37].

2.12. Detection of apoptotic cells from nuclear staining

The apoptotic cell populations were evaluated by staining cell nucleus with the DNA binding dye Hoechst 33258 (Sigma, USA) to assess the chromatin condensation through fluorescence microscopy [38, 39]. Cells were treated and washed with PBS and fixed in 1:1 acetomethanol (acetone: methanol) for 1 hr at 4 °C. These cells were then incubated with 1 mM Hoechst dye in PBS in the dark at room temperature for 5 mins. Excess stain was washed off with PBS and cells were observed under fluorescence microscope (AxioScope AI of Carl Zeiss).

2.13. Assessment of mitochondrial membrane potential ($\Delta\Psi mt$)

Changes in the mitochondrial membrane potential ($\Delta\Psi mt$) were determined using flow cytometry, FACS Calibur (BD Biosciences, USA) as described earlier [40]. Treated cells were washed in PBS, trypsinized and stained with 10 μg/ml JC-1 dye (Sigma, USA). After that, stained cells were incubated at 37 °C for 30 mins in dark. The mitochondrial depolarization was estimated by determining the number of cells that shifted from red to green fluorescence, in a flow cytometry (FACS Calibur, BD Biosciences, USA), after staining with JC-1dye, 10,000 cells per sample were analyzed [41]. For fluorescence microscopic analysis, the treated cells were also incubated with 2 μg/ml JC-1 dye in PBS for 20 mins in 37 °C as described in [42]. The cells were then observed under the fluorescence microscope (Invitrogen EVOS FL Auto Cell Imaging System).

2.14. Detection of apoptosis from Annexin V-FITC staining

Staining cells with PI and Annexin V-FITC can be used as a measure of apoptotic population. Following treatment protocol as above, cells were processed for determining cellular apoptosis through flow cytometry (BD Biosciences, USA) using Annexin V-FITC Apoptosis kit (Invitrogen) as described in [43]. This assay was done following instructions protocol of the kit manufacturer.

2.15. Western blot experiment

The expression of Bax was determined in exponentially growing A375 cells by immunoblotting technique. This was performed essentially as described by Ghosh et al. [44]. α -tubulin was taken as the loading control. After treatment, cell pellet was washed with 1X ice cold PBS and resuspended in NP-40 lysis buffer (50 mM Tris-HCl pH 8, 150 mM NaCl, 1% NP-40) containing 1X cOmpletemini™ protease inhibitor (Roche) for 30 mins on ice, which was followed by centrifugation at 14,000 rpm. The protein content of the supernatant was determined by using Quick Start Bradford Protein Assay reagent (Bio-Rad); samples (80 μg of proteins) were run in 12% SDS polyacrylamide gel. After electrophoresis, the gel was blotted onto a PVDF membrane (Bio-Rad) at room temperature, 80 V for 2 hrs for dry transfer (Blot Boy mini instrument; Benchmark). The membrane was then blocked with 5% BSA (Sigma) for 2 hr at 4 °C. After blocking, the membrane was incubated with α –tubulin (Cell Signaling Technology) antibody for 1 hr at room temperature in 1:1000 dilutions. Then, the membrane was washed thrice with 1X TBST (0.1% Tween20 in 1X TBS) and subsequently incubated with horseradish peroxidase (HRP) conjugated anti-Rabbit antibody (1:5000 dilutions) for 1 hr at room temperature. The membrane was finally washed thrice with 1X TBST and developed with enhanced chemiluminescence (ECL) solution and photographed in Bio-Rad XRS+. The membrane was then stripped in mild stripping buffer (200 mM glycine, 0.1% SDS, 1% Tween20), blocked and reprobed with rabbit Bax (Santa Cruz Biotechnology; dilution 1:1000) antibody for 1 hr at room temperature followed by same procedure till developing in ECL solution and finally photographed in Bio-Rad XRS+. ImageJ software was used for band density quantification.

2.16. Hoechst efflux studies

Hoechst efflux assay was carried out to evaluate the effect of ACPH on cancer stem cells. The side population of CSCs in the cell cultures are capable of effluxing chemotherapeutic drugs and chemicals [45]. The population of cancer stem cells is often evaluated through estimation of effluxing of Hoechst dye from a cancer cell culture. The method followed is essentially as described by Addla et al. [46]. In this experiment, verapamil treatment (50 and 75 μg/ml, 15 mins) at 37 °C was used as positive control. All treated cells were washed in PBS, incubated with Hoechst 33342 dye (Sigma, USA) at a final concentration of 5 μg/mL in 1×10^6 cells for 45 mins in water bath at 37 °C. Cells were gently agitated every 15 mins. The cells were then washed in cold PBS once and resuspended in pre-warmed (37 °C) medium and incubated for 45 mins for efflux. Data was collected in FACS Calibur (BD Biosciences, USA) [47].

2.17. Statistical analysis

Each experiment was repeated at least three times. The results are the mean ± SD (determined from Graphpad Prism 5.0 software). The statistical significance was calculated with ANOVA (Bonferroni's Post Hoc Test) at $P < 0.05$, the result was considered to be statistically significant.

3. Results and discussions

3.1. DNA photo-cleavage experiments

In vitro photo-cleavage assay is an important indicator for the photosensitizing activity of any dye. The photosensitizing action of dyes like Oxovanadium (IV) complexes, meloxicam complexes of Co(II) and Zn(II), b-carboline-bisindole compounds on UV or visible light exposure have been demonstrated through DNA photo-cleavage assay by other investigators [30, 48, 49]. For *in vitro* photo-cleavage experiment, pUC19 DNA was treated with ACPH alone, or exposed to UVA irradiation either alone or after exposure to ACPH. Closed circular conformation of plasmid DNA migrates faster in electrophoresis gel. If one strand is cleaved, a slower moving nicked confirmation (Form II) is produced from the supercoiled DNA (Form I), while a linear confirmation will be generated if both strands are cleaved. A typical agarose gel electrophoresis pattern is shown in Figure 1 (the uncropped micrograph of this gel is shown in the supplementary figure S1). Molecular marker DNA was loaded in lane 5; untreated control pUC19 DNA, the same DNA treated with ACPH (8 μM), UVA (15 KJ/m^2) without or with ACPH pretreatment were loaded in lanes 1–4 respectively; the relative intensities of the Form II to Form I bands of the plasmid DNA did not increase on ACPH treatment alone compared to that in the control. This relative intensity increased on exposure to UVA. This increase was more pronounced when the plasmid DNA was irradiated after ACPH treatment, indicating the *in vitro* photosensitizing action of ACPH.

3.2. Morphological observation

We have earlier observed from cellular uptake assay that ACPH is easily taken up by the cells within 1 hr (data not shown here). The morphological changes in cells on treatment with a nontoxic concentration of ACPH (2 μM) either alone or in combination with UVA (15 KJ/m^2) were therefore visualized. Cells treated with this concentration of ACPH exhibited no visible changes in morphology compared to controls, in both A375 and HEK 293 cells. Morphological changes in A375 cells were evident on UVA irradiation, the extent of damage was however greater in ACPH pretreated A375 cells. The change in cellular morphology due to such treatments was negligible in normal human HEK 293 cells. These observations are shown in Figure 2A. It indicated that the combined treatment of ACPH+UVA was more effective in causing damage to cancer cells than in normal cells. Morphological alterations also have been observed with other photosensitizers like benz(e)acephenanthrylene [50], quinine [51] on UVA irradiation in A375 cells. The morphology of A375 cells were also visualized under SEM which is shown in Figure 2B. No alteration in cellular morphology was found in cells treated with ACPH alone compared to control cells. Cellular disintegrity, membrane disruption with wrinkled and curled appearances were evident on UVA exposure, both, with or without ACPH pretreatment, in A375 cells. The effects were pronounced in the ACPH+UVA treated cells. Occurrence of apoptosis following low dose of PDT with erythrosine treatment and necrosis with high doses have been observed under SEM in both H357 and DOK cell lines [52]. Therefore, the effect of ACPH and UVA treatments on viability of cells was investigated.

3.3. Cell viability

Figure 3 shows the effect of pretreatment with a nontoxic dose of ACPH on UVA induced cytotoxicity in A375 and HEK 293 cells. It was observed that in A375 cells, treatment with ACPH prior to UVA exposure sensitized the cells to killing compared to that by UVA alone at all doses. For the same doses, UVA showed lower toxicity in HEK 293 cells, while pretreatment with ACPH had little effect on this killing. ACPH also sensitizes in both A549 human lung epithelial and B16 murine melanoma cell line to killing (results not shown here). Similar finding was found with ofloxacin and UVA [53]. 2-Aryl Benzothiazoles and 2-(4-aminophenyl) benzothiazole derivative with UVA light also showed greater cell killing potential than UVA irradiation alone in A375 and basal cell carcinoma (BCC) cells respectively [54, 55]. Some active acridine derivatives pentyl-AcrDIM and hexyl-AcrDIM also showed photocytotoxic effect towards the mouse lymphocytic leukemia cell line L1210 and human ovarian cancer cells A2780 while exhibiting lower toxicity in normal HaCaT cells [11].

3.4. Scratch assay

To explore the cellular growth inhibitory effect of a combined treatment of ACPH with UVA, the gap-closure or wound healing assay was performed in A375 cells. It was found that ACPH+UVA could inhibit regrowth of cells in the scratched area. Typical snapshots of control and treated cells exposed to UVA (15 KJ/m^2) with or without ACPH (2 μM) treatment are shown in Figure 4. It was found that cellular regrowth was significantly reduced in ACPH+UVA treated cells compared to the other sets of cells. There was complete regrowth of cells in the scratched area by 48 hrs in control and in cells treated only with ACPH. A significant decrease in cellular regrowth was observed in the scratched area for UVA irradiated cells, while almost no regrowth was observed in ACPH+UVA treated cells. Compounds like 1- benzothiazolyl phenyl benzotriazole in combination with UVA also significantly inhibited the migration and invasion of Ca9-22 cells which indicated the minimization of cell metastasis [56]. Other photosensitizer like ALA was however, unable to inhibit regrowth; cells migrated and invaded more effectively on such treatments [57].

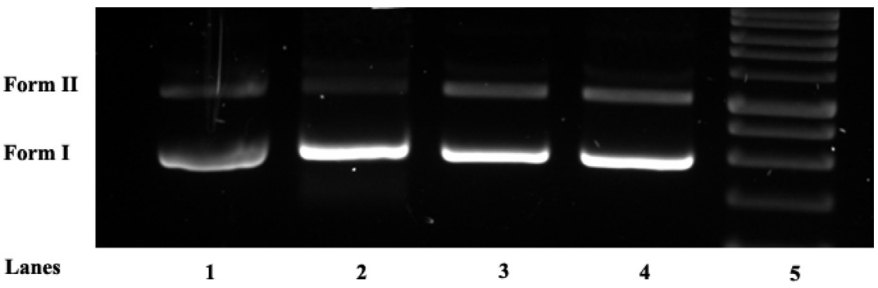

Figure 1. Photo-cleavage assay through agarose gel electrophoresis showing that ACPH pretreatment enhances the UVA light-induced cleavage of pUC19 DNA. Lane 1- pUC19 DNA, lane 2- DNA treated with ACPH (8 μM), lane 3- DNA exposed to UVA (15 KJ/m^2), lane 4- pUC19 DNA treated with ACPH (8 μM) prior to UVA exposure (15 KJ/m^2) and lane 5- marker DNA.

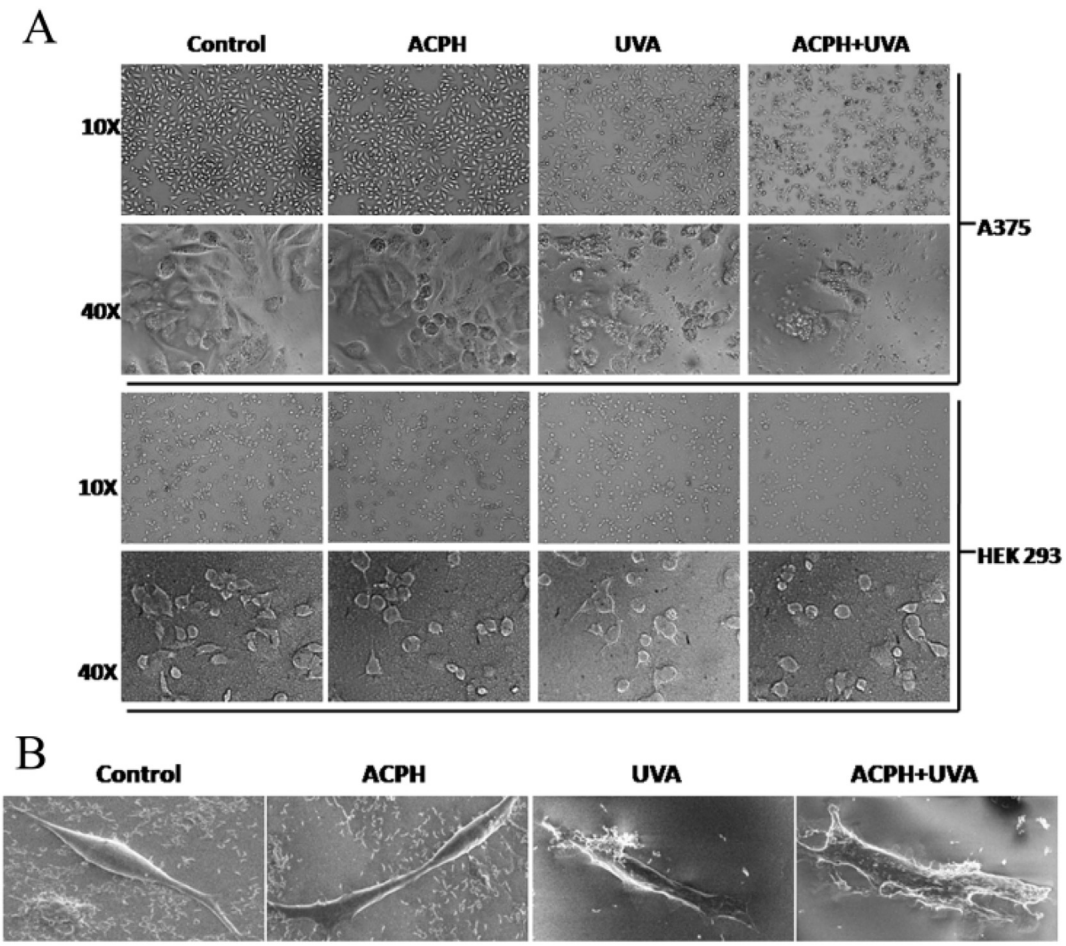

Figure 2. Comparison of morphological features between control and treated human melanoma A375 cells and in normal human embryonic kidney HEK 293 cells. A. The top two panels represent control, ACPH (2 μM, 1hr) treated and on UVA irradiation (15 KJ/m^2) with or without ACPH (2 μM) pretreatment for A375 cells under phase contrast light microscope at 10x and 40x magnifications. The lower two panels are for the same treatments in HEK 293 cells. B. A375 cells with the same treatment observed under SEM.

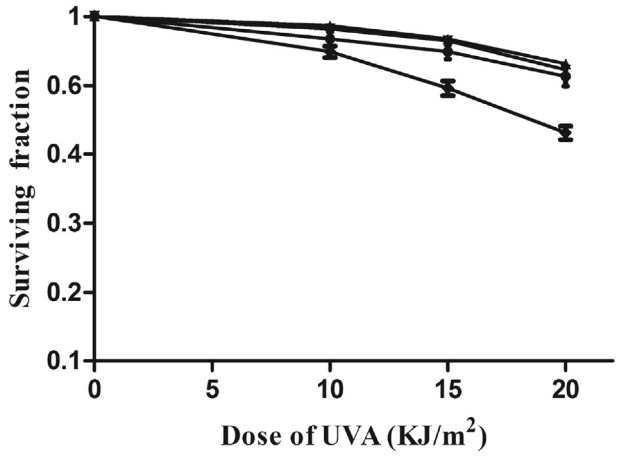

Figure 3. Influence of ACPH (2 μM) on viability of cells exposed to different doses of UVA for MTT assay. In A375 cells, with (-◆-) and without (-●-) ACPH and in HEK 293 cells with (-▼-) and without (-▲-) ACPH.

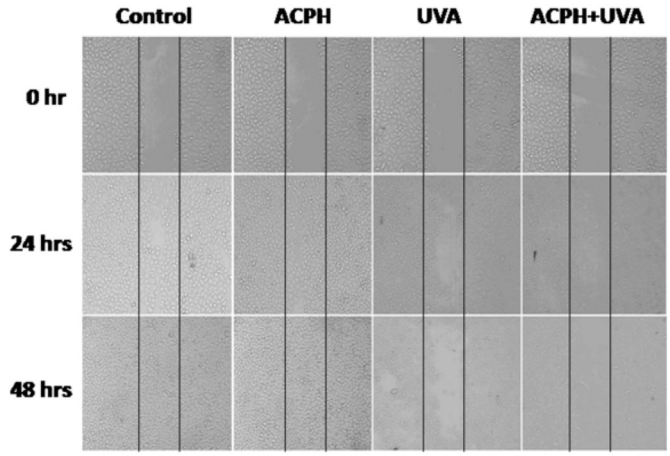

Figure 4. Effect of prior treatment of ACPH (2 μM) with UVA (15 KJ/m^2) radiation on scratch assay. Snapshots of the scratch areas for various time points (0, 24 and 48 hrs) after infliction were observed in A375 treated cells with respect to untreated cells through a phase contrast microscope (10x).

3.5. Determination of intracellular ROS level

Photosensitizers often involve oxidation reaction, which increases the generation of ROS in cells [58]. The ROS then initiate free radical chain reaction that are responsible for cell killing [59, 60]. Generation of cytotoxic ROS has thus been associated with the mechanism of action for several photosensitizers. Phototoxicity of UVA radiation was enhanced on anthracene, quinine or benz(e)acephenanthrylene treatment through the production of ROS [50, 51, 61, 62]. It was important to know whether

generation of ROS was involved in the cell killing process during ACPH associated photosensitization of UVA. Using DCFH-DA probe, the production of intracellular ROS was assessed both-microscopically and through flow cytometry. Figure 5A shows the fluorescence due to the generation of ROS within the cells on UVA (15 KJ/m^2) treatment with or without prior treatments with ACPH (2 μM). The fluorescence from cells treated with ACPH alone was not significantly different from that in control cells; this indicated that ACPH alone does not produce any ROS. Production of ROS was indicated through increase in fluorescence in UVA exposed cells; the fluorescence was even higher when cells were pretreated with ACPH. Similar finding was revealed from the flow cytometric assay, the results of which are shown in Figure 5B.

3.6. Determination of intracellular GSH level in cell

Intracellular antioxidant molecules like GSH control the redox homeostasis and counter the ROS generation in cells. Such events can cause depletion in intracellular GSH level [63]. An increase in PDT-induced cytotoxicity following GSH depletion has been reported [64]. Depletion of intracellular GSH by benz(e)acephenanthrylene plus UVA was observed in A375 cells [50]. Intracellular GSH level was also reduced by buthionine sulfoximine (BSO) in MDA-MB-231 cells [64]. The total cellular soluble thiol was determined to assess the GSH content in A375 cells on treatment with ACPH (2 μM) prior to UVA (15 KJ/m^2) irradiation. Table 1 shows the effect of pretreatment with ACPH after UVA exposure on the GSH level in A375 cells. There was no change in ACPH treated cells compared to that in control cells. Treatment with ACPH plus UVA resulted in a slight decrease in the GSH content in the cells which was found to be insignificant.

3.7. DNA damage assay by flow cytometry

UVA irradiation causes oxidative damage leading to DNA strand breakages. Binding of some ligands to DNA can result in enhancing this damage [65]. We assessed the effect of UVA on DNA damage with or without ACPH pretreatment through flow cytometric assay. The histogram plots of DNA content of cells have two peaks representing cells with 2n and 4n amount of DNA i.e., cells at G_1/S and at G_2/M phase. Cells with DNA damage have hypodiploid DNA content. H_2O_2 is known to generate oxygen free radicals which are involved in DNA damage in cells that cause mutagenesis. Therefore, H_2O_2 (600 μM, 1 hr) was used here as the positive control. ACPH (2 μM) alone did not induce any DNA damage in A375 cells. An increase in hypodiploid population was observed on UVA (15 KJ/m^2) exposure indicating DNA damage. The extent of DNA damage was higher, if the cells were treated with ACPH prior to irradiation. The results are shown in Figure 6. Such enhancement of DNA damage was found with other photosensitizers like2-(4-aminophenyl) benzothiazole derivatives and phthalocyanine in BCC and MCF-7c3 cells respectively [55, 66].

3.8. Lipid peroxidation assay

Photodynamic inactivation of cells is not just mediated through DNA damage, but it occurs through its cooperative effect on the immune system and its assault on lipids and proteins through ROS production [67]. MDA is the final product of polyunsaturated fatty acid peroxidation in the cells. Free radicals are normally responsible for the lipid peroxidation process in an organism which causes overproduction of MDA that is commonly known as a marker of oxidative stress. Lipid peroxidation has been used also as a marker of oxidative stress and the antioxidant status in cells [68]. ACPH (2 μM) treatment alone resulted in lowering the level of MDA formed in cells compared to that of control (Table 2). Exposure to UVA (15 KJ/m^2) increased the MDA formation, but ACPH (2 μM) pretreatment increased it further, indicating enhancement of oxidative damage in such cells. Chlorpromazine also is known to increase damage to membrane via lipid peroxidation with low doses of UVA [22]. PDT with Photofrin II also induced lipid peroxidation, which was accompanied by protein damage in A549 cells [69].

3.9. Determination of cell cycle by flow cytometry

Cell cycle arrest is generally associated with DNA damage. Recovery of cells leads to reversal of the cell cycle arrest, while severely damaged cell proceeds towards cell death. The percentage of cells in the different phases of cell cycle was determined through PI staining at different times (0, 6, 16 and 24 hrs) after exposure to UVA (15 KJ/m^2) radiation with or without ACPH (2 μM) pretreatment in A375 cells. This is represented through histogram plots in Figure 7. UVA alone induced cell cycle arrest at G_1/S phase. DNA damaging agents generally induce arrest at G_1 phase to facilitate DNA repair before

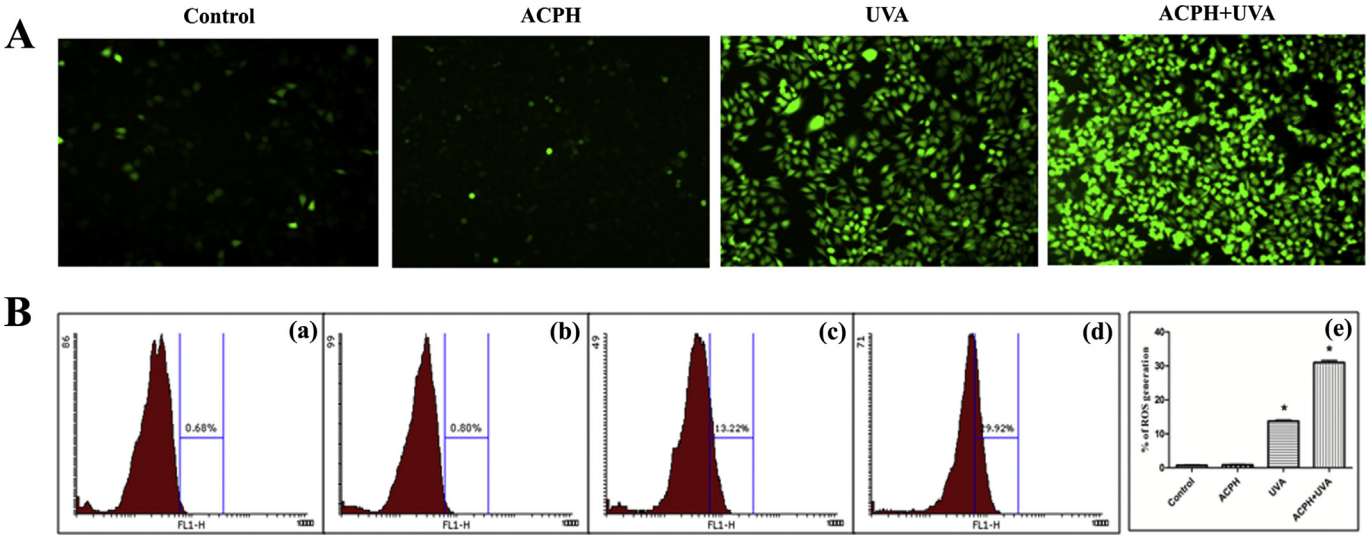

Figure 5. Estimation of ROS generated using DCFH-DA in A375 cells. A. Representative photographs showing control, ACPH (2 μM) treated and UVA (15 KJ/m^2) irradiated cells with or without ACPH pretreatment observed under fluorescence microscope. B. Typical histogram plots showing generation of ROS in A375 cells from flow cytometric assay using DCFH-DA (a) control cells, (b) ACPH (2 μM) treated, on UVA (15 KJ/m^2) exposure (c) alone and (d) with ACPH (2 μM) pretreatment before irradiation. (e) Bar diagram showing the increase in the percentage of ROS in treated cells. The data are represented as mean ± SD (n = 3) analyzed by one-way ANOVA (*P < 0.0001).

Table 1. Changes in cellular GSH level in A375 cells on UVA irradiation with or without ACPH pretreatment.

Treatment	GSH (ng/μg protein)	Fold increase
Control	0.231 ± 0.0195	1
ACPH	0.225 ± 0.1273	0.97
UVA (15 KJ/m^2)	0.192 ± 0.105	0.83
ACPH + UVA (15 KJ/m^2)	0.164 ± 0.0568	0.71

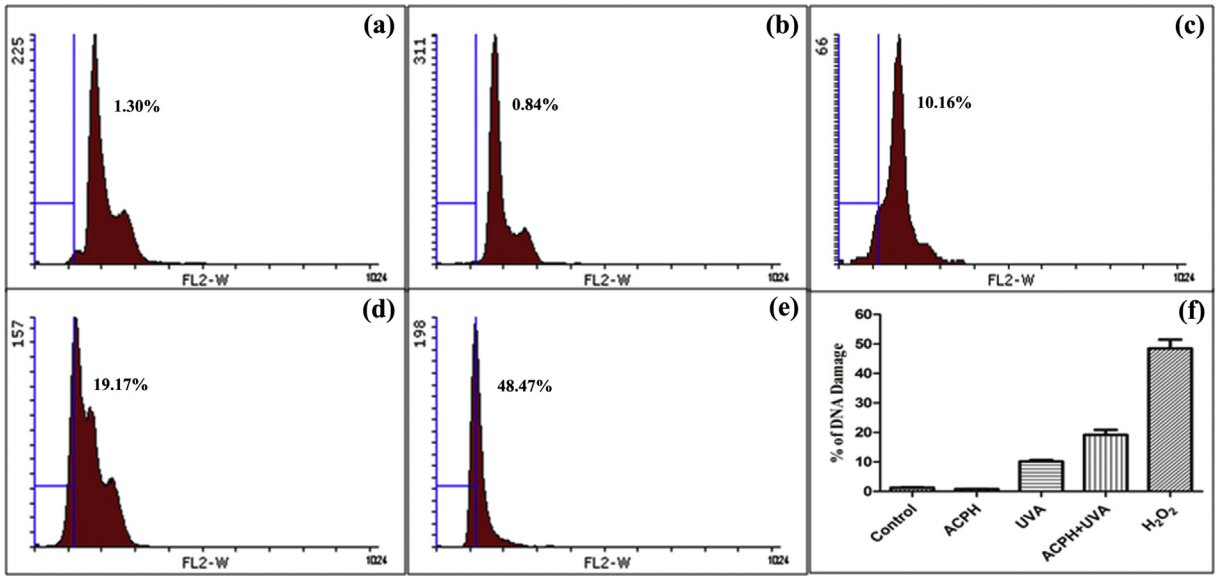

Figure 6. Effect of prior treatment of ACPH (2 μM) with UVA radiation on DNA damage through flow cytometry with PI staining. A typical histogram of PI-stained A375 cells showing the effect of pretreatment of ACPH with UVA radiation from flow cytometry of (a) control cells, (b) ACPH treated cells, (c) cells exposed to UVA (15 KJ/m^2) without and (d) with ACPH pretreatment, (e) H_2O_2 (600 μM for 1 hr) as a positive control; (f) bar diagram showing percent DNA damage for the above treatment. The data are represented as mean ± SD (n = 3), analyzed by one-way ANOVA (*P < 0.0001).

Table 2. MDA formed in A375 cells on UVA irradiation with or without ACPH pretreatment.

Treatment	MDA formed in A375 cells (nmol h^{-1} 10^{-6} cells)	Fold increase
Control	23.25 ± 4.0	1
ACPH	18.45 ± 2.4*	0.79
UVA (15 KJ/m^2)	29.64 ± 4.0025*	1.28
ACPH + UVA (15 KJ/m^2)	36.06 ± 4.0125*	1.55

The data are represented as mean ± SD (n = 3), analyzed by one-way ANOVA (*P < 0.0001).

duplication. In HaCaT cells, a significant increase of cells at G_1 phase was observed due to inhibition of progression in cell cycle at G_1/S phase through p^{53} independent mechanism [62]. Treatment with ACPH prior to UVA exposure resulted in an increase in G_2/M population with time. Levofloxacin and ofloxacin induced UVA mediated cell cycle arrest in G_2/M phase in HaCaT cells leading to the induction of apoptotic pathway [53, 70]. Timetrioxane 97/78 with UVB played a pivotal role in G_2/M cell arrest to induce apoptosis [71]. Photosensitization by anthrone with UVA also induced arrest at both S and G_2/M phases of cell cycle with concomitant decrease in G_1 phase in HaCaT cells [72]. Ketoprofen and mefloquine with UVB light too, led to the cell cycle arrest in G_2/M phase in HaCaT cells [73, 74]. The photosensitizer, quinine could also induce cell cycle arrest in G_2 phase on UVA exposure to decrease proliferation of A375 cells [51]. Increase in G_2/M population with time indicated arrest of cells in this phase. Permanent arrest can lead to cell death.

3.10. Detection of autophagy

Autophagy is a dynamic process which involves the transport of different cellular organelles and proteins through a lysosomal degradation pathway. It plays an important role in cell survival, differentiation, and development. Chemotherapeutic drugs or different anticancer stimuli can induce autophagy in various cancer cells [75]. It has been reported that PDT too, can induce autophagy [76]. The process of autophagy starts with the autophagosome formation and then formation of autophagolysosomes with the fusion of acidic lysosomes with autophagosomes. AVOs are considered to be indicative of autophagy. Here, we employed AO which accumulates in the lysosomes and emits bright red fluorescence, the intensity of which is proportional to the degree of the AVOs acidity and the volume of these structures. Fluorescence microscope was used to visualize the AVOs (red fluorescence) as well as the cytoplasm and nucleus (green fluorescence) after the vital staining of the cells with AO under 40x. Figure 8A depicts the induction of autophagy in

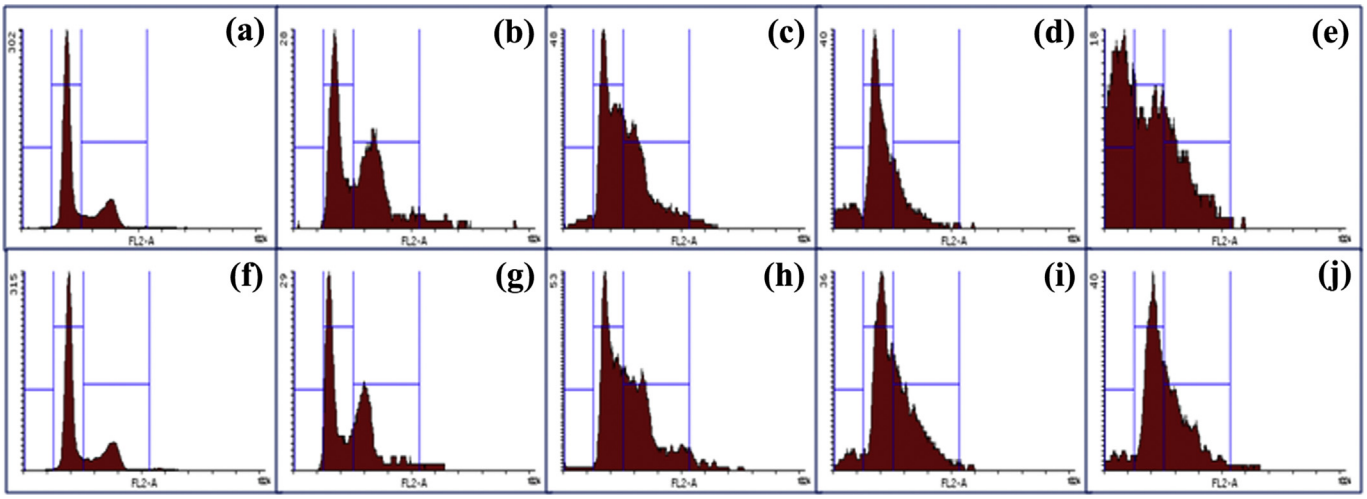

Figure 7. Cell cycle distribution in A375 cells through flow cytometry with PI staining. Typical histogram plots of cell cycle distribution in (a) control, (f) ACPH (2 μM) treated cells and after exposure to UVA (15 KJ/m^2) alone at (b) 0, (c) 6, (d) 16, and (e) 24 hrs, and with ACPH (2 μM) pretreatment at (g) 0, (h) 6, (i)16 and (j) 24 hrs.

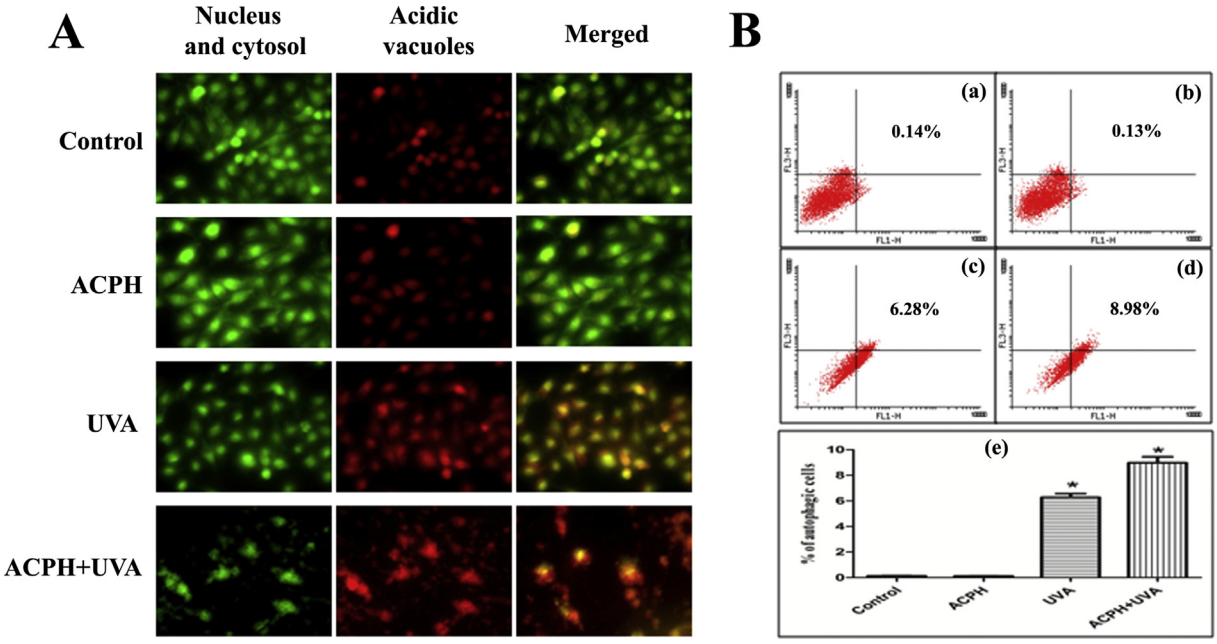

Figure 8. Estimation of intracellular autophagy in A375 cells through AO dye. A. The uptake of dye in cells observed under the fluorescence microscope for control, ACPH (2 μM) treated and UVA (15 KJ/m^2) irradiated without or with ACPH pretreatment. B. Flow cytometric assay after AO staining in (a) control, (b) ACPH treated, (c) on UVA (15 KJ/m^2) exposure alone and (d) on ACPH pretreatment before irradiation; (e) bar diagrams showing the percent fluorescence on different treatments from flow cytometric analysis. Data are represented as mean ± SD (n = 3) analyzed by one-way ANOVA (*P < 0.0001).

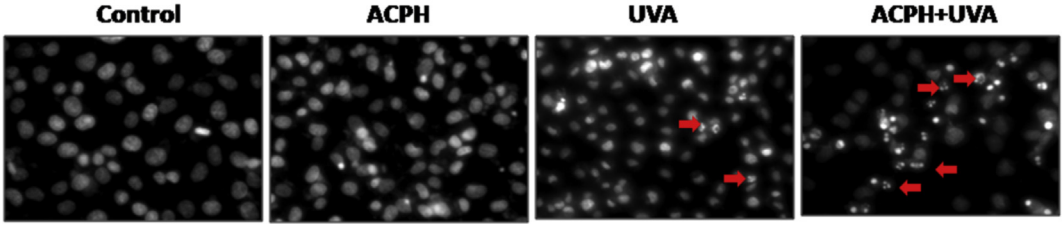

Figure 9. Micronuclei formation in A375 cells detected with Hoechst (33258) staining under fluorescence microscope in control, ACPH (2 μM) treated, and on UVA (15 KJ/m^2) exposure without or with ACPH (2 μM) pretreatment.

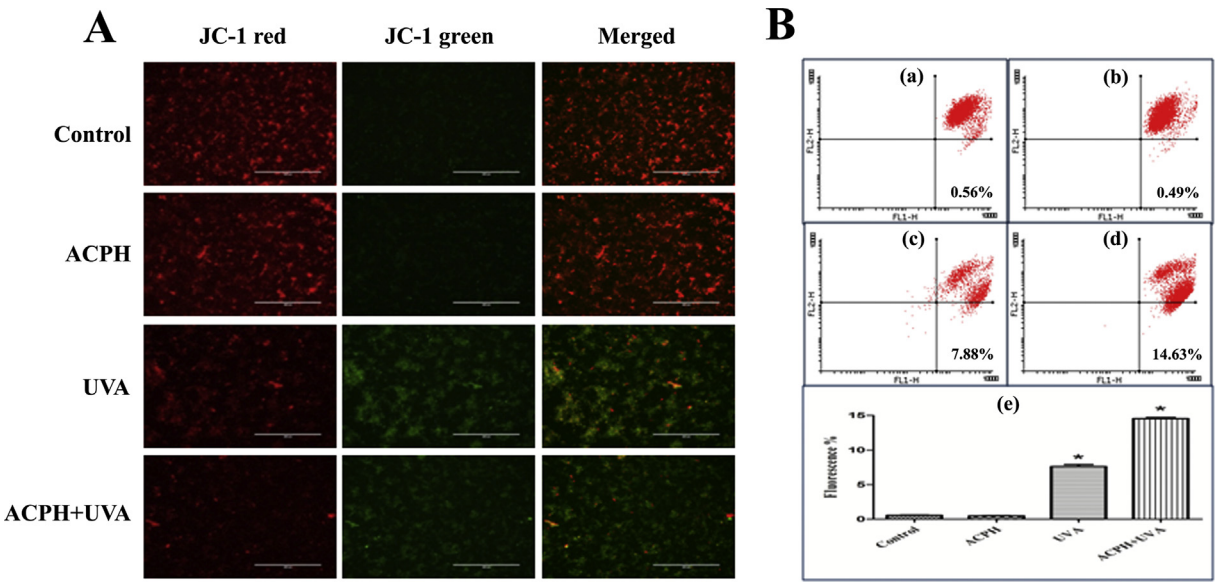

Figure 10. Estimation of depletion in mitochondrial membrane potential (ΔΨmt) in A375 cells through JC-1 dye uptake. A. The uptake of dye in cells observed under the fluorescence microscope for control, ACPH (2 μM) treated and UVA (15 KJ/m^2) irradiated without or with ACPH pretreatment. B. Flow cytometric assay of ΔΨmt in (a) control, (b) ACPH treated, (c) on UVA (15 KJ/m^2) exposure alone and (d) on ACPH pretreatment before irradiation; (e) bar diagrams showing the percent fluorescence on different treatments from flow cytometric analysis. Data are represented as mean ± SD (n = 3) analyzed by one-way ANOVA (*P < 0.0001).

A375 cells while the number of autophagic cells in control and ACPH were negligible; few autophagic cells were found on UVA (15 KJ/m^2) exposure and this number increased slightly in cells on pretreatment with ACPH (2 μM) prior to irradiation. Autophagic death was also quantified from flow cytometric assay using AO dye as depicted in Figure 8B. Both control and only ACPH treated cells showed no such accumulation of bright red fluorescence. There was a small increase in fluorescence from irradiated cells which was slightly enhanced on ACPH pretreatment, indicating a small increase in autophagic death. Sasnauskiene et al. showed that safranin-mediated PDT induced autophagy in A431 cells [77]. 5-ALA-PDT mediated autophagic cell death was also found in PC12 and CL1-0 cells where mitogen activated protein kinases (MAPKs) pathway played an important role in that process [78]. Cells exposed with UVB along CDRI-97/78 also exhibited a slight increase in green fluorescence in HaCaT cells to indicate more AVOs formation [71]. Some studies have shown that the lysosome plays a pivotal role in cell apoptosis

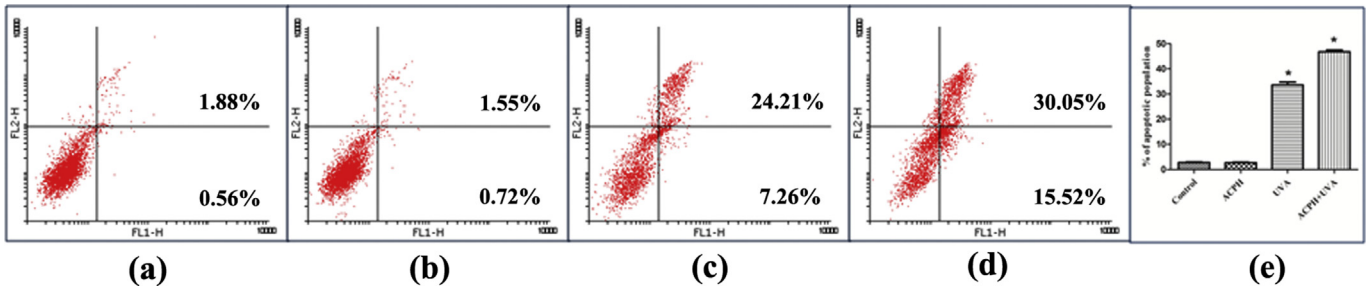

Figure 11. Detection of apoptosis in A375 cells from Annexin V-FITC staining through flow cytometry (a) control, (b) ACPH treated (2 μM), (c) on UVA (15 KJ/m^2) exposure and (d) with ACPH pretreatment before exposure; (e) bar diagram showing the increase in the percentage of apoptotic cells. Data are represented as mean ± SD (n = 3) analyzed by one-way ANOVA (*P < 0.0001).

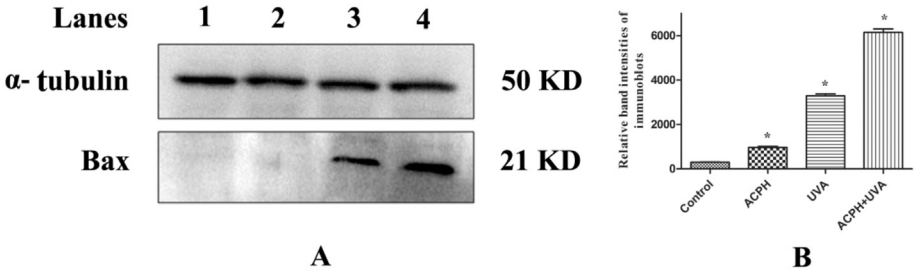

Figure 12. Expression of Bax in A375 cells from Western blotting. A. A typical micrograph showing Bax and α-tubulin expression in control, ACPH (2 μM) treatment and UVA (15 KJ/m^2) alone and with ACPH pretreatment before irradiation. α-tubulin was the loading control. B. Bar diagram showing the percentage of Bax expression for this treatment. Data are represented as mean ± SD (n = 3) analyzed by one-way ANOVA (*P < 0.0001).

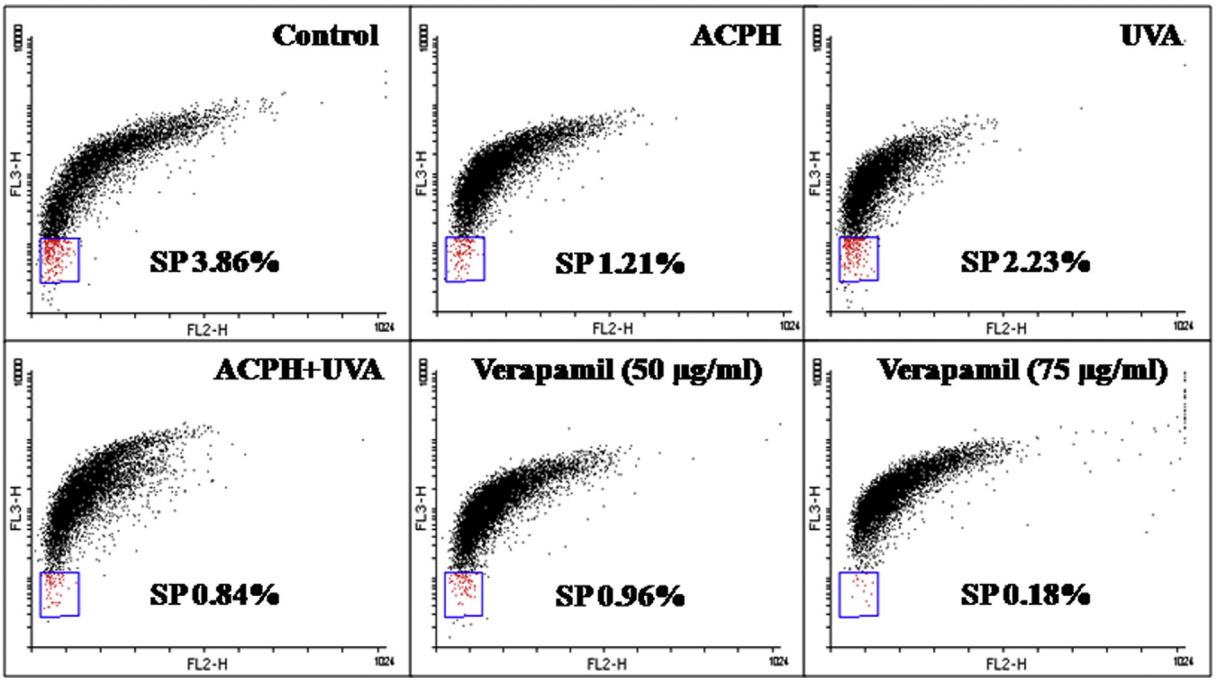

Figure 13. Effect on CSCs side population in A375 cells using Hoechst (33342) efflux assay in flow cytometer in control, ACPH (2 μM) treated, UVA (15 KJ/m^2) irradiated and on irradiation after ACPH (2 μM) pretreatment of cells. Verapamil (50, 75 μg/ml) was used as a positive control.

via mitochondrial dependent pathway which may lead to mitochondrial depolarization and lysosomal destabilization in cells due to up-regulation of Bax gene expression [72, 79]. Ofloxacin with UVA light also destabilized lysosomal integrity in HaCaT cells [53].

3.11. Detection of apoptotic cells from nuclear staining

Apoptosis is morphologically identified by cell shrinkage, chromatin condensation, inter-nucleosomal fragmentation, membrane blebbing, and cleavage of chromosomal DNA. Such hallmarks that characterize apoptosis were visualized in UVA (15 KJ/m^2) exposed A375 cells with or without ACPH (2 μM) pretreatment, using the fluorescent Hoechst (33258) dye to visualize the cellular nuclei. From Figure 9, it can be seen that no nuclear fragmentation was evident in control or ACPH treated cells, but UVA exposure without or with ACPH exhibited all such characteristics, which are indicated by arrows in the micrographs. It is discernible that greater chromatin condensation was observed in the cells treated with ACPH+UVA than in the cells treated with UVA alone. Such increase in chromatin condensation was observed in A2780 cells treated with the acridine derivative AcrDIM with UVA [11]. Combination treatment of ofloxacin with UVA also exhibited chromatin condensation in HaCaT cells [53].

3.12. Assessment of mitochondrial membrane potential (ΔΨmt)

Decrease in the mitochondrial membrane potential is a key mediator for initiation of apoptosis [54]. The decline in the mitochondrial membrane potential is an irreversible step, which marks the early event in the process of apoptosis. Mefloquine, a photosensitizer was found to induce apoptotic death in cells on irradiation [74]. Mitochondrial depolarization was observed in A375 cells treated with Ketoprofen and UVB light [73]. Treatment with Rose Bengal, followed by UVB and UVA exposures also led to decrease in mitochondrial membrane potential as well as translocation of phosphatidylserine from inner to outer plasma membrane in A375 cells [80]. Decrease in mitochondrial membrane potential can be visualized from the decrease in fluorescence intensity from cells bound to JC-1 and also quantified through flow cytometry. There was a decrease in the mitochondrial depolarization patterns of cells as indicated through a shift in red (J-aggregates) to green fluorescence (JC-1 monomers) in UVA (15 KJ/m^2) exposed cells pretreated with ACPH (2 μM), which was greater than that from cells irradiated with UVA alone (Figure 10A). The flow cytometric findings are shown in Figure 10B which also corroborated the same finding. While ACPH alone showed no difference in ΔΨmt from that in control cells, there is decrease in ΔΨmt in UVA irradiated cells. This was more pronounced in ACPH pretreated cells. These findings suggested the involvement of mitochondria mediated apoptosis in cell killing.

3.13. Detection of apoptosis from Annexin V-FITC staining

Apoptosis is a physiological mechanism of cell death, which is often exploited for elimination of malignant cells. Staining with Annexin V-FITC and PI was done to evaluate induction of apoptosis in A375 cells, the results of which are shown in Figure 11. There was no significant difference in the percent apoptotic population between the control and the cells treated with ACPH alone, an increased number of Annexin V-FITC and PI positive cells were observed in ACPH+UVA irradiated cells compared to cells exposed to UVA alone. Apoptotic death significantly increased to 45.57% on ACPH+UVA treatment compared to cells exposed only to UVA (31.47%), indicating that the photosensitization with ACPH can significantly enhance apoptotic death. Trioxane 97/78 with UVB radiation and ofloxacin with UVA also indicated apoptosis in HaCaT cells [53, 71].

3.14. Western blot experiment

Mitochondria mediated intrinsic apoptosis is modulated by the Bcl-2 family proteins. Bcl-2 family is broadly classified into three functional groups- the antiapoptotic proteins such as Bcl-2, proapoptotic effectors like Bax, and proapoptotic activators such as BH3 [81]. One of the proapoptotic proteins of the Bcl-2 family is Bax. In healthy cells, Bax is located in the cytoplasm, but during apoptosis, it is translocated to the

mitochondria to initiate apoptosis. Chiu et al. have shown that Bax is very important for mitochondria mediated apoptosis in PDT [66]. UVA radiation on photosensitization with ofloxacin showed upregulation of the proapoptotic gene Bax with no noticeable changes in the anti-apoptotic Bcl-2 protein [53]. Anthrone with UVA also upregulated the Bax mRNA expression that leads to apoptosis in keratinocytes [72]. Ketoprofen and mefloquine with UVB too, upregulated Bax in HaCaT cells [73, 74]. Rose Bengal followed by UVB and UVA exposures increased the Bax expression to induce apoptotic cell death in A375 cells [80]. We had checked the expression of Bax after pretreatment with ACPH (2 μM) on UVA (15 KJ/m^2) exposure. From Figure 12, it can be seen that the expression of Bax is upregulated in ACPH sensitized UVA treated A375 cells to affirm the role of mitochondria mediated cell death pathway. (The uncropped gel micrographs showing the expression of Bax and that for α-tubulin, as the control housekeeping protein are shown in the supplementary figure S2).

3.15. Hoechst efflux studies

Recent studies have suggested that there exists a small side populations of CSCs in tumors that are often resistant to treatment and are responsible for tumor progression and its recurrence in patients [82, 83]. The CSCs have the ability to strongly efflux the Hoechst dye (33342) by ABC membrane transporter. Effect of Hoechst efflux is therefore, taken as the indication of the existence of CSCs in a population of cancer cells. It was therefore, significant to explore if ACPH could have any effect on killing of the CSCs population. The findings from Hoechst efflux assay are shown in Figure 13.

Verapamil generally blocks the ABC membrane transporter from extruding the Hoechst dye. Two concentrations of verapamil (50 and 75 μg/ml) were used as the positive control. It can be seen that, ACPH alone could also reduce the efflux of the dye compared to that in control A375 cells; this was reduced significantly on ACPH+UVA treatment. The findings indicated that ACPH as a photosensitizer with UVA treatment could significantly reduce the side population of CSCs in A375 cells. The side population of CSCs can have a major role in metastasis. Our finding could be indicative of the ability of ACPH+UVA treatment in elimination of the CSCs. This may be of pivotal importance for its therapeutic activity.

4. Conclusion

Overall, our results suggested that nontoxic dose of ACPH with UVA light can inhibit proliferation of A375 cells by inducing DNA damage both in *in vitro* DNA and in cells through photosensitization. Such treatment enhanced the generation of ROS in cells leading to lipid peroxidation and depletion of GSH. This led to cell cycle arrest at G_2/M phase to promote apoptosis through mitochondria mediated pathway. Although, there was a slight increase in the small population of cells undergoing death through autophagy by UVA on ACPH pretreatment, primarily UVA+ACPH resulted in cell death through apoptosis. Thus, use of ACPH as a photosensitizer in PDT may be contemplated. Applying ACPH topically to target cell and then illuminating them with UVA, the concern of inducing damage to the surrounding normal cells can be minimised. Moreover, the ability of this combination to eliminate the stem cell population is highly encouraging and bolsters ACPH as a promising new photosensitizer, reinforcing its role as an anticancer agent.

Declarations

Author contribution statement

S Hansda: Conceived and designed the experiments; Performed the experiments; Analyzed and interpreted the data; Wrote the paper.

R. Ghosh: Conceived and designed the experiments; Analyzed and interpreted the data; Wrote the paper.

G. Ghosh: Contributed reagents, materials, analysis tools or data.

Funding statement

This work was supported by infrastructural facilities at the Department of Biochemistry and Biophysics, University of Kalyani (K.U.), funded by K.U. and from Department of Science & Technology- Fund for Improvement of S&T Infrastructure (DST-FIST), Promotion of University Research and Scientific Excellence of Department of Science & Technology (DST-PURSE) and Grants Commission-Special Assistance Programme (UGC-SAP), Govt. of India (GoI.) S. Hansda was supported by a fellowship from University Grants Commission-The Rajiv Gandhi National Fellowship (UGC-RGNF), GoI.

Competing interest statement

The authors declare no conflict of interest.

Additional information

Supplementary content related to this article has been published online at https://doi.org/10.1016/j.heliyon.2020.e04733.

Acknowledgements

Authors are thankful to Dr. Utpal Basu, Department of Molecular Biology and Biotechnology, K.U., for providing his laboratory facilities in some experiments.

References

[1] C.R. Caffrey, D. Steverding, R.K. Swenerton, B. Kelly, D. Walshe, A. Debnath, Y.M. Zhou, P.S. Doyle, A.T. Fafarman, J.A. Zorn, K.M. Land, J. Beauchene, K. Schreiber, H. Moll, A. Ponte-Sucre, T. Schirmeister, A. Saravanamuthu, A.H. Fairlamb, F.E. Cohen, J.H. McKerrow, J.L. Weisman, B.C.H. May, Bis-acridines as lead antiparasitic agents: structure-activity analysis of a discrete compound library in vitro, Antimicrob. Agents Chemother. 51 (2007) 2164–2172.
[2] S.A. Lyakhov, Y.I. Suveyzdis, L.A. Litvinova, S.A. Andronati, S.L. Rybalko, S.T. Dyadyun, Biological active acridine derivatives. Part 4: synthesis and antiviral activity of some bis-acridinylated diamides, Pharmazie 55 (2000) 733–736.
[3] M. Wainwright, Acridine—a neglected antibacterial chromophore, J. Antimicrob. Chemother. 47 (2001) 1–13.
[4] D. Greenwood, Conflicts of interest: the genesis of synthetic antimalarial agents in peace and war, J. Antimicrob. Chemother. 36 (1995) 857–872.
[5] M. Demeunynck, Antitumour acridines, Expert Opin. Ther. Pat. 14 (2004) 55–70.
[6] R. Ghosh, S. Bhowmik, D. Guha, 9-phenyl acridine exhibits antitumour activity by inducing apoptosis in A375 cells, Mol. Cell. Biochem. 361 (2012) 55–66.
[7] S. Bhowmik, A. Bagchi, R. Ghosh, Molecular modelling studies of some 9-arylacridines to elucidate their possible roles in Topoisomerase I inhibition, Int. J. Integr. Biol. 2 (2008) 8–14.
[8] S. Karmakar, D. Manna, S. Ghosh, S. Hansda, A. Bagchi, R. Ghosh, 9-Phenyl Acridine : a possible poly (ADP-ribose) polymerase-1 inhibitor, J. Chem. Pharm. 9 (2017) 188–200.
[9] S. Karmakar, R. Ghosh, New aryl derivatives of acridine with poly (ADP- ribose) polymerase 1 inhibitory activity: a molecular modeling approach, Int. J. Sci. Res. 4 (2015) 1362–1366.
[10] S. Karmakar, R. Ghosh, Synergistic action of Cisplatin and 9-Phenyl acridine in A375 cells 55 (2018) 173–182.
[11] L. Čižeková, A. Grolmusová, Z. Ipóthová, Z. Barbieriková, V. Brezová, L. Hunáková, J. Imrich, L. Janovec, I. Dovinová, H. Paulíková, Novel 3,6-bis(imidazolidine)acridines as effective photosensitizers for photodynamic therapy, Bioorg. Med. Chem. 22 (2014) 4684–4693.
[12] J. Rupar, V. Dobričić, J. Grahovac, S. Radulović, Ž. Skok, J. Ilaš, M. Aleksić, J. Brborić, O. Čudina, Synthesis and evaluation of anticancer activity of new 9-acridinyl amino acid derivatives, RSC Med. Chem. 11 (2020) 378–386.
[13] J. Chen, J.X. Zhao, Upconversion nanomaterials: synthesis, mechanism, and applications in sensing, Sensors 12 (2012) 2414–2435.
[14] R. Ghosh, S. Bhowmik, A. Bagchi, D. Das, S. Ghosh, Chemotherapeutic potential of 9-phenyl acridine: biophysical studies on its binding to DNA, Eur. Biophys. J. 39 (2010) 1243–1249.
[15] E. Marta Nagy, L. Dalla Via, L. Ronconi, D. Fregona, Recent advances in PUVA photochemotherapy and PDT for the treatment of cancer, Curr. Pharm. Des. 16 (2010) 1863–1876.
[16] P. Zhang, M.X. Wu, A clinical review of phototherapy for psoriasis, Lasers Med. Sci. 33 (2018) 173–180.
[17] B.P. Group, British photodermatology group guidelines for PUVA, Br. J. Dermatol. 130 (1994) 246–255.

[18] A.M. del, Porphyrins, porphyrias, cancer and photodynamic therapy - a model for carcinogenesis, J. Photochem. Photobiol. B Biol. 20 (1993) 5–22.
[19] W. Kobayashi, Q. Liu, H. Nakagawa, H. Sakaki, B. Teh, T. Matsumiya, H. Yoshida, T. Imaizumi, K. Satoh, H. Kimura, Photodynamic therapy with mono-l-aspartyl chlorin e6 can cause necrosis of squamous cell carcinoma of tongue: experimental study on an animal model of nude mouse, Oral Oncol. 42 (2006) 45–49.
[20] T.J. Kinsella, E.D. Baron, V.C. Colussi, K.D. Cooper, C.L. Hoppel, S.T. Ingalls, M.E. Kenney, X. Li, N.L. Oleinick, S.R. Stevens, S.C. Remick, Preliminary clinical and pharmacologic investigation of photodynamic therapy with the silicon phthalocyanine photosensitizer Pc 4 for primary or metastatic cutaneous cancers, Front. Oncol. 1 (2011) 1–6.
[21] A.F. Dos Santos, D.R.Q. De Almeida, L.F. Terra, M.S. Baptista, L. Labriola, Photodynamic therapy in cancer treatment - an update review, J. Cancer Metastasis Treat. 2019 (2019).
[22] A. Wolnicka-Głubisz, B. Rajwa, J. Dobrucki, J. Skrzeczyńska-Moncznik, G.B. van Henegouwen, T. Sarna, Phototoxicity, distribution and kinetics of association of UVA-activated chlorpromazine, 8-methoxypsoralen, and 4,6,4′-trimethylangelicin in Jurkat cells, J. Photochem. Photobiol. B Biol. 78 (2005) 155–164.
[23] S.M. Fien, A.R. Oseroff, Photodynamic therapy for non-melanoma skin cancer, JNCCN J. Natl. Compr. Cancer Netw. 5 (2007) 531–540.
[24] Q. Sun, B.Y. Zheng, Y.H. Zhang, J.J. Zhuang, M.R. Ke, J.D. Huang, Highly photocytotoxic silicon(IV) phthalocyanines axially modified with L-tyrosine derivatives: effects of mode of axial substituent connection and of formulation on photodynamic activity, Dye. Pigment. 141 (2017) 521–529.
[25] H. Mirzaei, G.E. Djavid, M. Hadizadeh, M. Jahanshiri-Moghadam, P. Hajian, The efficacy of Radachlorin-mediated photodynamic therapy in human hepatocellular carcinoma cells, J. Photochem. Photobiol. B Biol. 142 (2015) 86–91.
[26] N. Hodgkinson, C.A. Kruger, M. Mokwena, H. Abrahamse, Cervical cancer cells (HeLa) response to photodynamic therapy using a zinc phthalocyanine photosensitizer, J. Photochem. Photobiol. B Biol. 177 (2017) 32–38.
[27] Y.Y. Huang, D. Vecchio, P. Avci, R. Yin, M. Garcia-Diaz, M.R. Hamblin, Melanoma resistance to photodynamic therapy: new insights, Biol. Chem. 394 (2013) 239–250.
[28] C.N. Honors, C.A. Kruger, H. Abrahamse, Photodynamic therapy for metastatic melanoma treatment: a review, Technol. Cancer Res. Treat. 17 (2018) 1–15.
[29] J.H. Lee, J.E. Kim, B.J. Kim, K.H. Cho, In vitro phototoxicity test using artificial skin with melanocytes, Photodermatol. Photoimmunol. Photomed. 23 (2007) 73–80.
[30] B. Banik, K. Somyajit, G. Nagaraju, A.R. Chakravarty, Oxovanadium(iv) complexes of curcumin for cellular imaging and mitochondria targeted photocytotoxicity, Dalt. Trans. 43 (2014) 13358–13369.
[31] W. Liu, X. Lu, G. He, X. Gao, M. Xu, J. Zhang, M. Li, L. Wang, Z. Li, L. Wang, C. Luo, Protective roles of Gadd45 and MDM2 in blueberry anthocyanins mediated DNA repair of fragmented and non-fragmented DNA damage in UV-irradiated HepG2 cells, Int. J. Mol. Sci. 14 (2013) 21447–21462.
[32] H.Y. Hsieh, W.C. Lee, G.C. Senadi, W.P. Hu, J.J. Liang, T.R. Tsai, Y.W. Chou, K.K. Kuo, C.Y. Chen, J.J. Wang, Discovery, synthetic methodology, and biological evaluation for antiphotoaging activity of bicyclic[1,2,3]triazoles: in vitro and in vivo studies, J. Med. Chem. 56 (2013) 5422–5435.
[33] R. Ghosh, D. Guha, S. Bhowmik, S. Karmakar, Some UV-bystander effects are mediated through induction of antioxidant defense in mammalian cells 49 (2012) 371–378.
[34] R. Ghosh, D. Guha, S. Bhowmik, UV released factors induce antioxidant defense in A375 cells, Photochem. Photobiol. 88 (2012) 708–716.
[35] M. Budzowska, I. Jaspers, J. Essers, H. De Waard, E. Van Drunen, K. Hanada, B. Beverloo, R.W. Hendriks, A. De Klein, R. Kanaar, J.H. Hoeijmakers, A. Maas, Mutation of the mouse Rad17 gene leads to embryonic lethality and reveals a role in DNA damage-dependent recombination, EMBO J. 23 (2004) 3548–3558.
[36] W. Peng, T. Du, Z. Zhang, F. Du, J. Jin, A. Gong, Knockdown of autophagy-related gene LC3 enhances the sensitivity of HepG2 cells to epirubicin, Exp. Ther. Med. 9 (2015) 1271–1276.
[37] T. Kanzawa, Y. Kondo, H. Ito, S. Kondo, I. Germano, Induction of autophagic cell death in malignant glioma cells by arsenic trioxide, Cancer Res 63 (2003) 2103–2108.
[38] Z. Ma, L. Hou, Y. Jiang, Y. Chen, J. Song, The endogenous oxindole isatin induces apoptosis of MCF-7 breast cancer cells through a mitochondrial pathway, Oncol. Rep. 32 (2014) 2111–2117.
[39] R. Ghosh, K. Girigoswami, D. Guha, Suppression of apoptosis leads to cisplatin resistance in V79 cells subjected to chronic oxidative stress, Indian J. Biochem. Biophys. 49 (2012) 363–370.
[40] D. Manna, R. Bhuyan, F. Saikh, S. Ghosh, J. Basak, R. Ghosh, Novel 1,4-dihydro-pyridine induces apoptosis in human cancer cells through overexpression of Sirtuin1, Apoptosis 23 (2018) 532–553.
[41] M. Salido, J.L. Gonzalez, J. Vilches, Loss of mitochondrial membrane potential is inhibited by bombesin in etoposide-induced apoptosis in PC-3 prostate carcinoma cells, Mol. Cancer Ther. 6 (2007) 1292–1299.
[42] G.R.S. Babu, T. Anand, N. Ilaiyaraja, F. Khanum, N. Gopalan, Pelargonidin modulates Keap1/Nrf2 pathway gene expression and ameliorates citrinin-induced oxidative stress in HepG2 cells, Front. Pharmacol. 8 (2017) 1–20.
[43] M.J. Akhtar, A.A. Siddiqui, A.A. Khan, Z. Ali, R.P. Dewangan, S. Pasha, M.S. Yar, Design, synthesis, docking and QSAR study of substituted benzimidazole linked oxadiazole as cytotoxic agents, EGFR and erbB2 receptor inhibitors, Eur. J. Med. Chem. 126 (2017) 853–869.
[44] T. Ghosh, U. Basu, Cis-acting sequence elements and upstream open reading frame in mouse utrophin-A 5′-UTR repress cap-dependent translation, PLoS One 10 (2015) 12–17.
[45] K. Moitra, H. Lou, M. Dean, Multidrug efflux pumps and cancer stem cells: insights into multidrug resistance and therapeutic development, Clin. Pharmacol. Ther. 89 (2011) 491–502.
[46] S.K. Addla, M.D. Brown, C.A. Hart, V.A.C. Ramani, N.W. Clarke, Characterization of the Hoechst 33342 side population from normal and malignant human renal epithelial cells, Am. J. Physiol. Ren. Physiol. 295 (2008) 680–688.
[47] T. Teramura, K. Fukuda, S. Kurashimo, Y. Hosoi, Y. Miki, S. Asada, C. Hamanishi, Isolation and characterization of side population stem cells in articular synovial tissue, BMC Musculoskelet. Disord. 9 (2008) 1–13.
[48] T.H. Sanatkar, H. Hadadzadeh, J. Simpson, Z. Jannesari, The meloxicam complexes of Co(II) and Zn(II): synthesis, crystal structures, photocleavage and in vitro DNA-binding, J. Mol. Struct. 1049 (2013) 336–344.
[49] J. Kovvuri, B. Nagaraju, V.L. Nayak, R. Akunuri, M.P.N. Rao, A. Ajitha, N. Nagesh, A. Kamal, Design, synthesis and biological evaluation of new β-carboline-bisindole compounds as DNA binding, photocleavage agents and topoisomerase I inhibitors, Eur. J. Med. Chem. 143 (2018) 1563–1577.
[50] D. Ali, R.S. Ray, R.K. Hans, UVA-induced cytotoxicity and DNA damaging potential of benz (e) acephenanthrylene, Toxicol. Lett. 199 (2010) 193–200.
[51] N. Yadav, A. Dwivedi, S.F. Mujtaba, H.N. Kushwaha, S.K. Singh, R.S. Ray, Ambient UVA-induced expression of p53 and apoptosis in human skin melanoma A375 cell line by quinine, Photochem. Photobiol. 89 (2013) 655–664.
[52] A.D. Garg, M. Bose, M.I. Ahmed, W.A. Bonass, S.R. Wood, In vitro studies on erythrosine-based photodynamic therapy of malignant and pre-malignant oral epithelial cells, PLoS One 7 (2012) 1–12.
[53] A. Dwivedi, S.F. Mujtaba, N. Yadav, H.N. Kushwaha, S.K. Amar, S.K. Singh, M.C. Pant, R.S. Ray, Cellular and molecular mechanism of ofloxacin induced apoptotic cell death under ambient UV-A and sunlight exposure, Free Radic. Res. 48 (2014) 333–346.
[54] Y.K. Chen, G.C. Senadi, C.H. Lee, Y.M. Tsai, Y.R. Chen, W.P. Hu, Y.W. Chou, K.K. Kuo, J.J. Wang, Apoptosis induced by 2-aryl benzothiazoles-mediated photodynamic therapy in melanomas via mitochondrial dysfunction, Chem. Res. Toxicol. 27 (2014) 1187–1198.
[55] W.P. Hu, Y.K. Chen, C.C. Liao, H.S. Yu, Y.M. Tsai, S.M. Huang, F.Y. Tsai, H.C. Shen, L. Sen Chang, J.J. Wang, Synthesis, and biological evaluation of 2-(4-aminophenyl) benzothiazole derivatives as photosensitizing agents, Bioorg. Med. Chem. 18 (2010) 6197–6207.
[56] G.C. Senadi, C.M. Liao, K.K. Kuo, J.C. Lin, L. Sen Chang, J.J. Wang, W.P. Hu, Design, synthesis and antimetastatic evaluation of 1-benzothiazolylphenylbenzotriazoles for photodynamic therapy in oral cancer cells, Medchemcomm 7 (2016) 1151–1158.
[57] J.M. Fahey, A.W. Girotti, Accelerated migration and invasion of prostate cancer cells after a photodynamic therapy-like challenge: role of nitric oxide, Nitric Oxide 49 (2015) 47–55.
[58] S.M. Mahalingam, J.D. Ordaz, P.S. Low, Targeting of a photosensitizer to the mitochondrion enhances the potency of photodynamic therapy, ACS Omega 3 (2018) 6066–6074.
[59] W. Bäumler, J. Regensburger, A. Knak, A. Felgenträger, T. Maisch, UVA and endogenous photosensitizers - the detection of singlet oxygen by its luminescence, Photochem. Photobiol. Sci. 11 (2012) 107–117.
[60] P.C. Chiang, R.H. Chou, H.F. Chien, T. Tsai, C.T. Chen, Chloride intracellular channel 4 involves in the reduced invasiveness of cancer cells treated by photodynamic therapy, Lasers Surg. Med. 45 (2013) 38–47.
[61] Z. Zhou, J. Song, L. Nie, X. Chen, Reactive oxygen species generating systems meeting challenges of photodynamic cancer therapy, Chem. Soc. Rev. 45 (2016) 6597–6626.
[62] S.F. Mujtaba, A. Dwivedi, M.K.R. Mudiam, D. Ali, N. Yadav, R.S. Ray, Production of ROS by photosensitized anthracene under sunlight and UV-R at ambient environmental intensities, Photochem. Photobiol. 87 (2011) 1067–1076.
[63] R. Reliene, R.H. Schiestl, Glutathione depletion by buthionine sulfoximine induces DNA deletions in mice, Carcinogenesis 27 (2006) 240–244.
[64] T.A. Theodossiou, C.E. Olsen, M. Jonsson, A. Kubin, J.S. Hothersall, K. Berg, The diverse roles of glutathione-associated cell resistance against hypericin photodynamic therapy, Redox Biol 12 (2017) 191–197.
[65] B. Epe, DNA damage spectra induced by photosensitization, Photochem. Photobiol. Sci. 11 (2012) 98–106.
[66] S.M. Chiu, L.Y. Xue, J. Usuda, K. Azizuddin, N.L. Oleinick, Bax is essential for mitochondrion-mediated apoptosis but not for cell death caused by photodynamic therapy, Br. J. Cancer. 89 (2003) 1590–1597.
[67] M. Sivasubramanian, Y.C. Chuang, L.W. Lo, Evolution of nanoparticle-mediated photodynamic therapy: from superficial to deep-seated cancers, Molecules 24 (2019).
[68] W.P. Gaweł S1, M. Wardas, E. Niedworok, Malondialdehyde (MDA) as a lipid peroxidation marker, Wiadomości Lek. 57 (2004) 9–10.
[69] J. Saczko, J. Kulbacka, A. Chwiłkowska, M. Lugowski, T. Banaś, Levels of lipid peroxidation in A549 cells after PDT in vitro, Rocz. Akad. Med. w Białymstoku. 49 (Suppl 1) (2004) 82–84.
[70] A. Dwivedi, S.F. Mujtaba, H.N. Kushwaha, D. Ali, N. Yadav, S.K. Singh, R.S. Ray, Photosensitizing mechanism and identification of levofloxacin photoproducts at ambient UV radiation, Photochem. Photobiol. 88 (2012) 344–355.
[71] A. Dwivedi, M.K. Pal, A.K. Tripathi, N. Yadav, S.F. Mujtaba, M.C. Pant, S.K. Singh, D.P. Mishra, R.S. Ray, B.H. Manjunatha Prabhu, Role of type-II pathway in apoptotic cell death induction by photosensitized CDRI-97/78 under ambient exposure of UV-B, Toxicol. Lett. 222 (2013) 122–131.
[72] S.F. Mujtaba, A. Dwivedi, N. Yadav, R.S. Ray, G. Singh, Singlet oxygen mediated apoptosis by anthrone involving lysosomes and mitochondria at ambient UV exposure, J. Hazard Mater. 252–253 (2013) 258–271.

[73] R.S. Ray, S.F. Mujtaba, A. Dwivedi, N. Yadav, A. Verma, H.N. Kushwaha, S.K. Amar, S. Goel, D. Chopra, Singlet oxygen mediated DNA damage induced phototoxicity by ketoprofen resulting in mitochondrial depolarization and lysosomal destabilization, Toxicology 314 (2013) 229–237.
[74] N. Yadav, A. Dwivedi, S.F. Mujtaba, A. Verma, R. Chaturvedi, R.S. Ray, G. Singh, Photosensitized mefloquine induces ROS-mediated DNA damage and apoptosis in keratinocytes under ambient UVB and sunlight exposure, Cell Biol. Toxicol. 30 (2014) 253–268.
[75] S. Fulda, Autophagy in cancer therapy, Front. Oncol. 7 (2017) 128.
[76] J.J. Reiners, P. Agostinis, K. Berg, N.L. Oleinick, D. Kessel, Assessing autophagy in the context of photodynamic therapy, Autophagy 6 (2010) 7–18.
[77] A. Sasnauskiene, J. Kadziauskas, N. Vezelyte, V. Jonusiene, V. Kirveliene, Apoptosis, autophagy and cell cycle arrest following photodamage to mitochondrial interior, Apoptosis 14 (2009) 276–286.
[78] H.T. Ji, L.T. Chien, Y.H. Lin, H.F. Chien, C.T. Chen, 5-ALA mediated photodynamic therapy induces autophagic cell death via AMP-activated protein kinase, Mol. Cancer. 9 (2010) 1.
[79] V. Stoka, B. Turk, S.L. Schendel, T.H. Kim, T. Cirman, S.J. Snipas, L.M. Ellerby, D. Bredesen, H. Freeze, M. Abrahamson, D. Brömme, S. Krajewski, J.C. Reed, X.M. Yin, V. Turk, G.S. Salvesen, Lysosomal protease pathways to apoptosis: cleavage of Bid, not pro-caspases, is the most likely route, J. Biol. Chem. 276 (2001) 3149–3157.
[80] A.K. Srivastav, S.F. Mujtaba, A. Dwivedi, S.K. Amar, S. Goyal, A. Verma, H.N. Kushwaha, R.K. Chaturvedi, R.S. Ray, Photosensitized rose Bengal-induced phototoxicity on human melanoma cell line under natural sunlight exposure, J. Photochem. Photobiol. B Biol. 156 (2016) 87–99.
[81] J. Marie Hardwick, L. Soane, Multiple functions of BCL-2 family proteins, Cold Spring Harb. Perspect. Biol. 5 (2013) 1–22.
[82] M.L.G., M.N. Craig, T. Jordan, Cancer stem cells, N. Engl. J. Med. 355 (2006) 1253–1261.
[83] L.L. Song, L. Miele, Cancer stem cells - an old idea that's new again: implications for the diagnosis and treatment of breast cancer, Expert Opin. Biol. Ther. 7 (2007) 431–438.